Giant reversible magnetocaloric effect in MnNiGe-based materials

Minimizing thermal hysteresis via crystallographic compatibility modulation

Liu, Jun; Gong, Yuanyuan; You, Yurong; You, Xinmin; Huang, Bowei; Miao, Xuefei; Xu, Guizhou; Xu, Feng; Brück, Ekkes

DOI
10.1016/j.actamat.2019.05.066

Publication date
2019

Document Version
Final published version

Published in
Acta Materialia

Acta Materialia 174 (2019) 450–458

Contents lists available at ScienceDirect

Acta Materialia

journal homepage: www.elsevier.com/locate/actamat

Full length article

Giant reversible magnetocaloric effect in MnNiGe-based materials: Minimizing thermal hysteresis via crystallographic compatibility modulation

Jun Liu [a, b], Yuanyuan Gong [a, *], Yurong You [a], Xinmin You [b], Bowei Huang [b], Xuefei Miao [a], Guizhou Xu [a], Feng Xu [a, **], Ekkes Brück [b]

[a] MIIT Key Laboratory of Advanced Metallic and Intermetallic Materials Technology, School of Materials Science and Engineering, Nanjing University of Science and Technology, Nanjing 210094, People's Republic of China
[b] Fundamental Aspects of Materials and Energy (FAME), Delft University of Technology, Mekelweg 15, 2629 JB Delft, the Netherlands

ARTICLE INFO

Article history:
Received 15 April 2019
Received in revised form
27 May 2019
Accepted 30 May 2019
Available online 1 June 2019

Keywords:
Magnetocaloric effect
Magnetostructural transformation
Thermal hysteresis
Reversibility
Geometrically nonlinear theory of martensite

ABSTRACT

MnMX (M = Co or Ni, X = Si or Ge) alloys with strong magnetostructural coupling exhibit giant magnetic entropy change and are currently extensively studied. However, large thermal hysteresis results in serious irreversibility of the magnetocaloric effect in this well-known system. In this work, we report a low thermal hysteresis and large reversible magnetocaloric effect in a MnNiGe-based system. The introduction of Fe into both Ni and Mn sites can establish stable magnetostructural transitions from paramagnetic hexagonal to ferromagnetic orthorhombic phases. Fascinatingly, a low thermal hysteresis of 5.2 K is achieved in $Mn_{0.9}Fe_{0.2}Ni_{0.9}Ge$ alloy with a large magnetization difference of 62.1 A m^2/kg between the two phases. These optimized parameters lead to a partially reversible phase transformation under a magnetic stimulus and bring about a large reversible magnetic entropy change of −18.6 $Jkg^{-1}K^{-1}$ under the field variation of 0–5 T, which is the largest value reported in MnMX system up to now. Moreover, this low-hysteresis magnetostructural transformation and large reversible magnetocaloric effect can be tuned by doping with Si in a wide temperature range covering room temperature. We also introduce geometrically nonlinear theory to discuss the origin of low hysteresis in MnMX alloys. A strong relation is found between thermal hysteresis and the change of *c* axis in the orthorhombic structure during the transition. Our work greatly develops the potential of MnMX alloys as magnetocaloric materials and is meaningful to seek or design a MnMX system with low thermal hysteresis.

1. Introduction

Due to the environmental friendliness and high theoretical energy efficiency, solid-state cooling is considered to be a promising alternative to conventional vapor compression refrigeration that uses strong greenhouse or flammable gases [1–3]. Since the discovery of giant magnetocaloric effect (MCE) at room temperature [4], the ways to improve the performance of magnetocaloric materials has attracted increasing attention and magnetic refrigeration is becoming an active field in materials science. So far, several classes of first-order magnetostructural transformation (MST) systems, including Heusler-type Ni-Mn based alloys [5,6], $(Mn,Fe)_2(P,Si)$-based alloys [7,8], $Gd_5(Si_2Ge_2)$ [4], $La(Fe,Si)_{13}$-based compounds [9–11], and MnMX (M = Co or Ni, X = Si or Ge) compounds [12–14], have been reported to exhibit large MCE during the magnetic-field-induced MST. Among them, MnMX has been extensively investigated due to its strong coupling between magnetic and structural degrees of freedom [15,16]. MnMX experiences a tunable thermoelastic martensitic transformation from high-temperature Ni_2In-type hexagonal to low-temperature TiNiSi-type orthorhombic phase [13]. When the transformation temperature (T_t) is within the temperature region between the Curie-temperatures of orthorhombic and hexagonal phases (T^o_C and T^h_C), MST between the ferromagnetic (FM) orthorhombic and the paramagnetic (PM) hexagonal phase can be established [17]. The accompanied large magnetization difference (ΔM) between two phases is helpful for the magnetic-field-induced MST from

* Corresponding author.
** Corresponding author.
E-mail addresses: gyy@njust.edu.cn (Y. Gong), xufeng@njust.edu.cn (F. Xu).

https://doi.org/10.1016/j.actamat.2019.05.066
1359-6454/

hexagonal to orthorhombic phases, resulting in considerable MCE [17].

Since the magnetic cooling refrigerator is employed with periodic sweeps of cycles [18], the performance of magnetocaloric materials under cyclic exposure to magnetic fields is of great significance from the viewpoint of application. In MST material, the pronounced hysteretic phenomenon linked to the first-order transition leads to the functional degradation of MCE under magnetic cycles [19,20]. Therefore, to obtain a reversible magnetic-field-induced MST as well as the accompanied large MCE, the thermal hysteresis (ΔT_{hys}) should be as low as possible. In most MnMX alloys displaying MSTs, the values of ΔT_{hys} are as large as 10–30 K [12–16,21]. In that case, the magnetic-field-induced MST completely disappears during the second field cycle and the reversible entropy change under the magnetic field variation of 0–5 T is negligible [22]. Although replacing Mn by Fe can reduce ΔT_{hys} to be lower than 10 K [17], whether the MST can be reversibly induced by the cyclic magnetic field is ignored in most studies. On the other hand, the reason why substituting Fe for Mn decreases ΔT_{hys} remains unsolved.

Here, we choose MnNiGe as the starting material, which experiences an orthorhombic-hexagonal structural transformation at about 470 K and possesses a helical antiferromagnetic (AFM) state below 346 K [23,24]. Different from single-element substitution of Mn with Fe reported before, we introduce Fe into both Ni and Mn sites and realize a PM-FM-type MST. Fascinatingly, a low ΔT_{hys} of 5.2 K is observed in $Mn_{0.9}Fe_{0.2}Ni_{0.9}Ge$. Due to this optimization, the MST can be repeatedly induced by cyclic magnetic fields and a large reversible entropy change (ΔS_m) of about $-18.6\ Jkg^{-1}K^{-1}$ under the field change of 0–5 T is obtained. To the best of our knowledge, this is the largest reversible ΔS_m reported for MnMX alloys. We also investigate the origin of this low hysteresis based on crystallographic theory of martensite. Furthermore, the low-hysteresis MST as well as the large reversible MCE is not just present in this singular composition, but can be tuned by Si-doping in a wide temperature range covering room temperature.

2. Experimental

The polycrystalline samples with nominal composition of $Mn_{1-x}Fe_{2x}Ni_{1-x}Ge$ ($x = 0.02$, 0.04, 0.06, 0.08, 0.10, 0.12, 0.14, 0.16) were prepared by arc-melting high-purity raw materials under argon atmosphere for three times. The as-cast ingots were annealed in evacuated quartz tubes at 1073 K for five days, followed by quenching into water. The crystal structures of all samples were identified by powder X-ray diffraction (XRD) with Cu-$K\alpha$ radiation from Bruker D8 Advance at room temperature. For the temperature dependent XRD measurement, patterns were collected using a PANalytical X-pert Pro diffractometer equipped with an Anton Paar TTK450 low-temperature chamber. The structure refinement of the XRD patterns was performed using Fullprof's implementation of the Rietveld refinement method [25]. Microstructural determinations were performed by transmission electron microscope (TEM) and electron diffraction with a FEI TecnaiG2 20 LaB6TEM. The TEM sample was cut by focused ion beam (FIB). Elemental mapping images were also taken by energy-dispersive spectroscopy (EDS) in the scanning electron microscope (SEM, FEI Quanta 250F). To confirm T_t, differential scanning calorimetry (DSC) measurements were carried out using a Mettler Toledo DSC 3 with a heating/cooling rate of 10 K/min.

Magnetic measurements were performed using a cryogen-free physical property measurement system (PPMS Dynacool™) with a vibrating sample magnetometer from Quantum Design. The samples used for magnetic measurements are small bulk pieces of ~10 mg. Specifically, for isothermal magnetization (M-B) measurements around T_t, the so-called loop process was adopted to eliminate the influence of thermal history [26]: For each M-B curve, the sample was initially heated up to the complete hexagonal phase region. Then the sample was cooled slowly to the target temperature at 2 K/min. To guarantee the temperature stability of measurement, a waiting time of 300 s was held at the initial and target temperatures.

3. Results and discussion

3.1. The crystalline structures and microstructures

Stoichiometric MnNiGe alloy crystallizes with the orthorhombic structure (*Pnma*, space group 62) at room temperature [22,23]. When Mn and Ni are partially substituted by Fe (the specific atom occupation is shown in Supplementary Materials, Fig. S1), the relative stability of crystalline structures changes. Fig. 1a shows the room-temperature XRD patterns of $Mn_{1-x}Fe_{2x}Ni_{1-x}Ge$ system. For the samples with $x \leq 0.04$, the orthorhombic phase predominates. With increasing the substitution level, the intensity of peaks indexed as hexagonal phase ($P6_3/mmc$, space group 194) increases rapidly. For the sample with $x = 0.06$, both orthorhombic and hexagonal phases in coexistence are observed. When the substitution level further increases, only hexagonal phase is found. The selected area electron diffraction (SAED) pattern (Fig. 1b) for the sample with $x = 0.10$ also indicates a pure hexagonal structure. This pattern is consistent with the [201] zone axes of Ni_2In-type structure. The corresponding TEM micrograph is shown in Fig. 1c, where only a few dislocations are observed (marked by red circles). We confirm that our samples are highly homogeneous. As shown in EDS mapping (Fig. 1d), constituent elements distribute uniformly in the selected areas. Here, we only present the SEM and TEM data for the sample with $x = 0.10$, which exhibits the lowest ΔT_{hys} (shown below).

The evolution of structure suggests that T_t decreases to be lower than room temperature with the increase of x. It is well known that the TiNiSi-type orthorhombic structure is a distortion of the Ni_2In-type hexagonal structure and the reduction of a_o/b_o (c_h/a_h) ratio tends to stabilize the hexagonal structure (the lattice constants of the two structures are related to be: $a_o = c_h$, $b_o = a_h$ and $c_o = \sqrt{3}a_h$ [22]. The subscripts of o and h indicate orthorhombic and hexagonal structures, respectively) [27]. As shown in Fig. 1e, the value of a_o/b_o (c_h/a_h) decreases evidently with the increase of x, and it further reveals the decrease of T_t. As inferred from the information before, the decrease of T_t is beneficial to achieve the magneto-structural coupling.

3.2. The achievement of magnetostructural coupling

Temperature dependences of magnetization (M-T curves) under a high magnetic field of 5 T are shown in Fig. 2a. The reason for us to choose such a high magnetic field is to reflect how the saturation magnetization varies with temperature and substitution level. For the sample with $x = 0.02$, the structural transformation, manifested as the hysteretic magnetization discontinuity, occurs at about 380 K, which is higher than T^o_C (345 K). When $0.02 < x < 0.14$, T_t is reduced to be lower than 345 K, and the typical, sharp first-order MST between PM hexagonal and high-magnetization orthorhombic phase is observed. On further increasing x to 0.16 the structural transformation will vanish, leaving a smooth magnetic transition in the stable hexagonal phase. The suppression of the martensitic transition may be ascribed to the instability of the atom vibration at *2d* site in the parent phase caused by the FM order when the structural transition is tuned below T^h_C (the atom sites in Ni_2In-type structure is shown in Supplementary Materials, Fig. S1) [17,28]. Since stoichiometric MnNiGe alloy develops a helical AFM

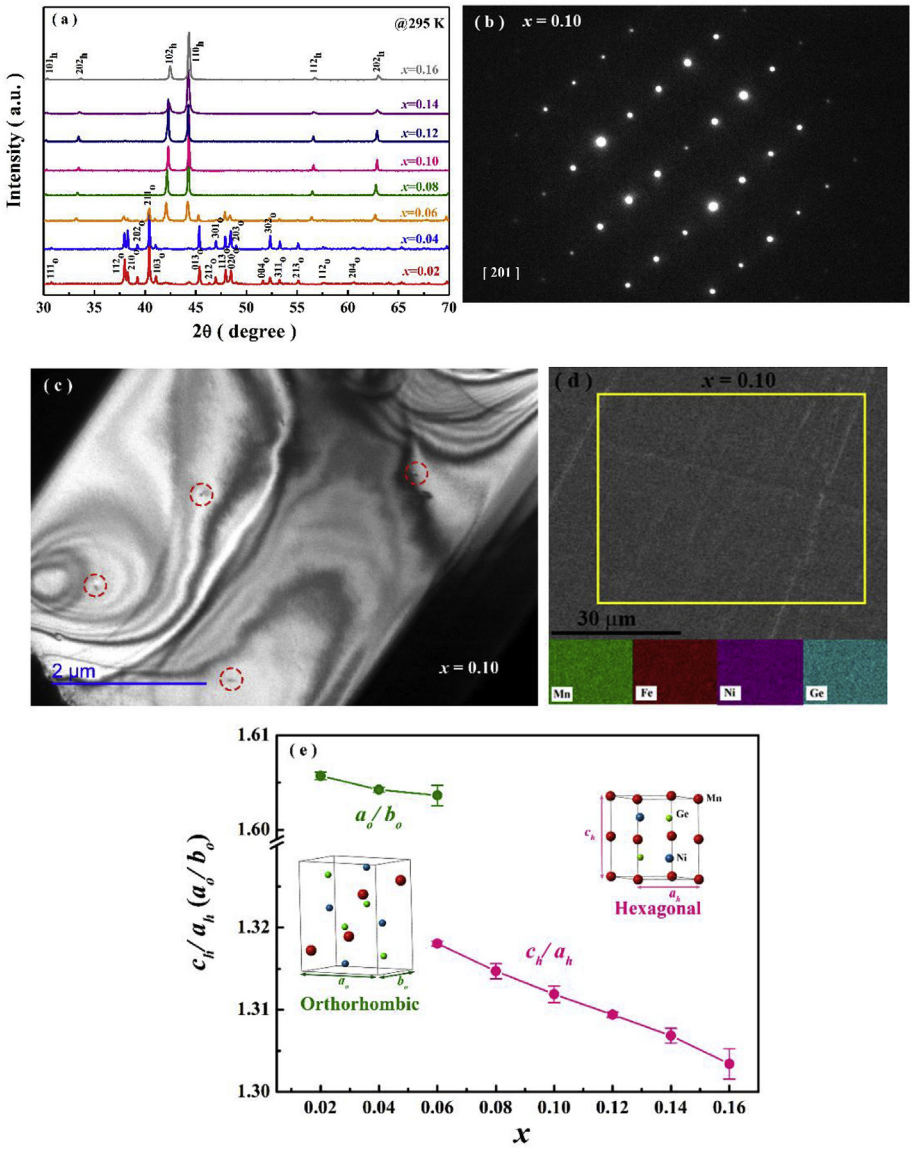

Fig. 1. (a) Powder XRD patterns for $Mn_{1-x}Fe_{2x}Ni_{1-x}Ge$ system at room temperature. (b) Electron diffraction patterns of a sample with $x = 0.10$ along [210] zone axis. (c) Bright field TEM micrographs. The dislocations are visible marked by red circles. (d) EDS mapping of selected area for sample with $x = 0.10$. (e) Ratio c_h/a_h (a_o/b_o) for $Mn_{1-x}Fe_{2x}Ni_{1-x}Ge$ system. Insets are the orthorhombic and hexagonal crystalline structures. (For interpretation of the references to colour in this figure legend, the reader is referred to the Web version of this article.)

state below the Néel temperature ($T^o_N = 346$ K) [23], the observed high-magnetization in the low-temperature orthorhombic phase is considerable. Fig. 2b shows M-B curves at 5 K. The magnetization of the sample with $x = 0.02$ shows a near-linear increase with the increase of magnetic field, which reflects the helical nature of antiferromagnetism [17]. With increasing x, a metamagnetic transition can be observed and the critical field decreases. While a FM behavior is observed in the sample $x = 0.14$. It implies that introducing Fe into both Ni and Mn sites not only reduces T_t but also changes the magnetic ground state, thus T^o_N gradually becomes T^o_C. This is because the introduction of magnetic Fe causes strong FM couplings of Fe-6Mn configurations out of the instable helical structures and leads to the collapse of AFM ordering [17]. Based on this improvement, a large ΔM of about 62.1 A m^2/kg is obtained in the sample with $x = 0.10$ (Fig. 2a), which is favorable in improving the MCE. Notably, the sample with $x = 0.16$ displays a lower saturation magnetization, which is ascribed to the stronger Mn-Mn coupling and wider 3*d* bandwidth from the closer Mn-Mn separation in the hexagonal phase [29].

Based on the M-T curves, the structural and magnetic phase diagram of $Mn_{1-x}Fe_{2x}Ni_{1-x}Ge$ system is obtained, as shown in Fig. 3. Here, T_t in the cooling (heating) sequence is defined as $(M_s + M_f)/2$ $((A_s + A_f)/2)$, where M_s, M_f, A_s and A_f correspond to the martensitic transformation start and finish temperatures, austenitic transformation start and finish temperatures, respectively (shown in Fig. 2a). These characteristic temperatures obtained from M-T curves are in accordance with those obtained from the DSC data (Fig. S2 in Supplementary Materials). In Fig. 3, it can be found that a large temperature interval of first-order MST from 175 to 345 K is established. In this temperature interval, MST between PM hexagonal and FM orthorhombic phase can be achieved. The width of this temperature interval is comparable to some other MnMX alloys, such as MnCoGe-based compounds, $Mn_{1-x}Fe_xNiGe$, $MnNi_{1-x}Fe_xGe$ and $Mn_{1-x}NiCo_xGe$ alloys [17,21,30].

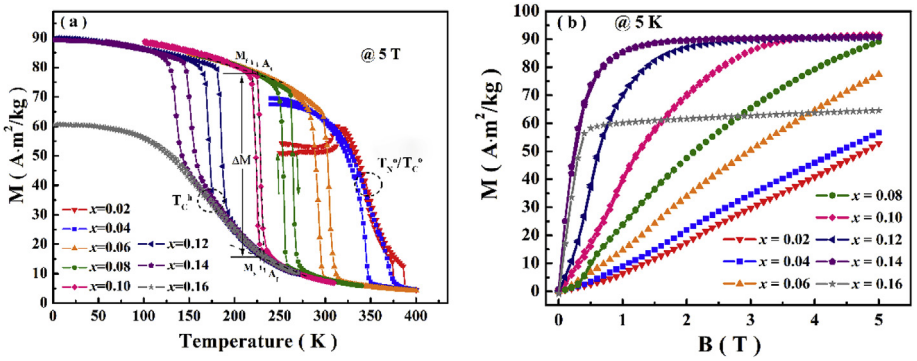

Fig. 2. (a) M-T curves under the field of 5 T during heating and cooling processes for $Mn_{1-x}Fe_{2x}Ni_{1-x}Ge$ system. The characteristic temperatures and ΔM are indicated in the graph. (b) M-B curves with increasing and decreasing magnetic fields at 5 K for $Mn_{1-x}Fe_{2x}Ni_{1-x}Ge$ system.

3.3. The composition optimization and magnetic-field-induced phase transition

According to Fig. 2a, it is worth noting that the sample with $x = 0.10$ displays a low ΔT_{hys} during the MST. The corresponding value obtained by T_t (heating) - T_t (cooling)) is 5.2 K. It is known that ΔT_{hys} is highly related to the method of calculating the T_t. Based on the differential curve of the M-T curve, the ΔT_{hys} is about 4.3 K (Fig. S3 in Supplementary Materials). Therefore, ΔT_{hys} of the sample with $x = 0.10$ is much lower than many other MnMX alloys [12–17,21,22,30]. Fig. 4a further shows the evolution of ΔT_{hys} and ΔM for the $Mn_{1-x}Fe_{2x}Ni_{1-x}Ge$ system. Both the lowest ΔT_{hys} and largest ΔM appear in the sample with $x = 0.10$, which is beneficial to achieve a large reversible MCE. To confirm the thermal stability of the observed low hysteresis, MST in the sample with $x = 0.10$ is checked under thermal cycles. As shown in Fig. 4b, the DSC curves under 28 cycles almost overlap and no significant shift of T_t is found, indicating the high thermal stability of the phase transformation and the related ΔT_{hys}. As compared with magnetic data, the slight deviation of T_t and ΔT_{hys} may arise from different heating/cooling rates and sample masses [31,32].

For MST materials, in analogy to the stimuli of temperature or stress, the magnetic field can also overcome the energy barrier between two phases and trigger a first-order MST. Fig. 4c shows the M-B curves of the sample with $x = 0.10$ in the magnetic field variation from 0 to 5 T. Around T_t, the magnetic-field-induced MST accompanied by a large magnetic hysteresis is seen, which indicates that the hexagonal phase tends to be transformed into the orthorhombic phase under a magnetic field. Additionally, a kink in the low field range of M-B curve is presented. This is attributed to the metamagnetic transition of the orthorhombic phase from the nonlinear magnetic structure to the high magnetization state. The magnetic-field-induced MST can also be observed by comparing the M-T curves measured under low and high magnetic field. Since the orthorhombic phase with higher magnetization is stabilized under a high magnetic field, T_t increases as shown in Fig. 4d.

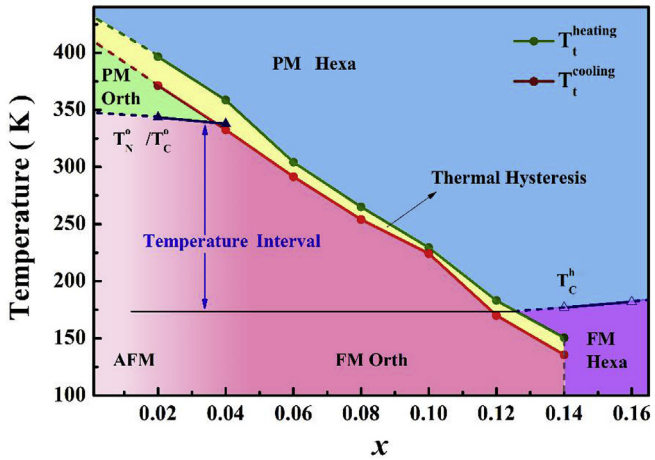

Fig. 3. Magnetic and structural phase diagram for $Mn_{1-x}Fe_{2x}Ni_{1-x}Ge$ system.

3.4. Magnetocaloric effect and its reversibility

The strong spin-lattice coupling always brings about a large MCE, in which the latent heat of the first-order transition plays a major role [7]. On the basis of the M-B curves, an important parameter on evaluating the MCE ΔS_m is calculated by using Maxwell relation:

$$\Delta S_m = \int_0^B \left(\frac{\partial M}{\partial T}\right)_B dB \tag{1}$$

Fig. 5a presents the temperature dependence of ΔS_m under different magnetic field variations for the sample with $x = 0.10$. As the field increases, a larger fraction of the transition would be involved, leading to the increase of ΔS_m and the shift of the peak. Under a low field change of 0–2 T, a maximum ΔS_m of -12.5 $Jkg^{-1}K^{-1}$ is observed. While under a field change of 0–5 T, the peak value reaches -39.6 $Jkg^{-1}K^{-1}$ which is larger than those reported for MnNiGe-based alloys by the same method [14,17,21,33,34].

However, it is controversial to achieve ΔS_m by Maxwell relations for first-order transition due to the spike effect [35]. Thus, the transformation mass fraction method (TF_MB) based on M-B curves is adopted to estimate ΔS_m of the sample with $x = 0.10$ [36–38]. The value is calculated by:

$$\Delta S_m = \Delta f \cdot \Delta S_t = \left(f\left(T, B_f\right) - f(T, B_i)\right) \cdot \Delta S_t \tag{2}$$

ΔS_t is the total entropy change of complete transition that can be estimated by DSC data [20]. And $f(T, B)$, the mass fraction of orthorhombic structure, can be given from the formula below by assuming the magnetization is proportional to the mass fraction of hexagonal and orthorhombic phases,

$$f(T, B) = \frac{M_{\exp}(T, B) - M_h(T, B)}{M_o(T, B) - M_h(T, B)} \tag{3}$$

where $M_{exp}(T, B)$ is the measured magnetization at a given

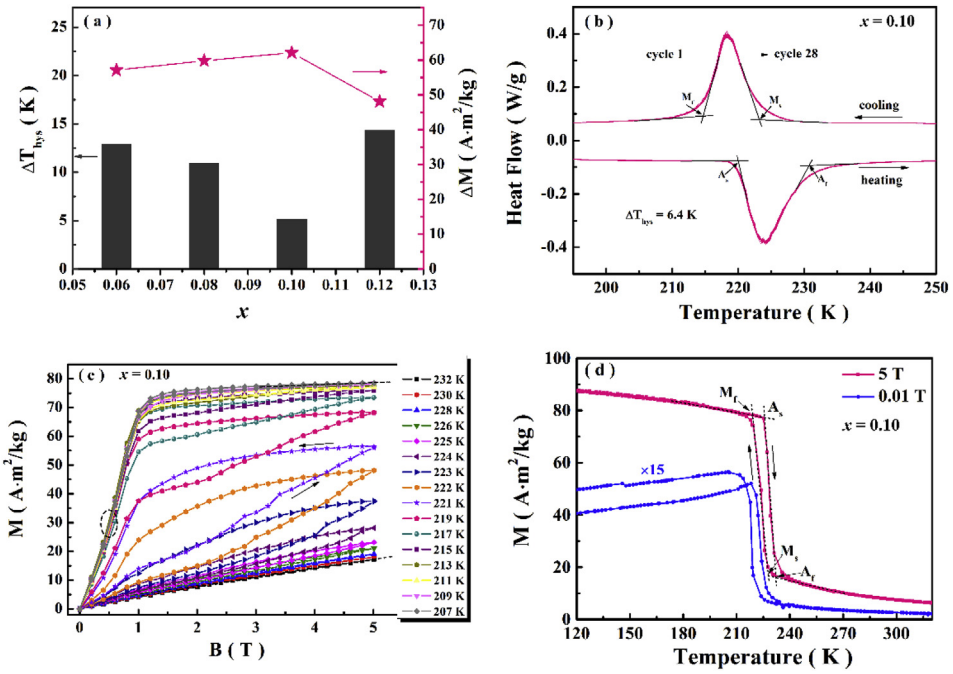

Fig. 4. (a) The ΔT_{hys} and ΔM for samples with $x = 0.06$, 008, 0.10 and 0.12. (b) DSC curves for optimized sample with $x = 0.10$ during thermal cycles. The characteristic temperatures are shown in the graph. (c) M-B curves measured in the vicinity of T_t with increasing and decreasing field for the sample with $x = 0.10$. The kinks representing the metamagnetic transition in low field are marked by the black circle. (d) M-T curves under the field of 0.01 and 5 T for the sample with $x = 0.10$. The curve under 0.01 T is enlarged to see the shift of T_t.

temperature and magnetic field shown in Fig. 4c. And $M_h(T, B)$ and $M_o(T, B)$ represent the magnetization of pure hexagonal and orthorhombic phases, respectively. It is well known that $M_o(T, B)$ of the ferromagnet depends on both the field and temperature [39]. Here, we only concentrate on the narrow temperature range around T_t where $M_o(T, B)$ just varies slightly (the details shown in Supplementary Materials, Fig. S4). Thus for simplicity, $M_o(T, B)$ is extracted from a linear extrapolation of the magnetization curve recorded at 207 K. Due to the rapid change of magnetization at low fields, the data below 1.0 T is excluded to guarantee the validity of the magnetization value. This approximation is also adopted to achieve the magnetization of the pure hexagonal structure with PM state which is determined by linearly extrapolating the M-B curve at 232 K. Based on this, the field dependence of the mass fraction of the orthorhombic phase at different temperatures are calculated and shown in Fig. 5b. Combined with ΔS_t that is calculated to be about -57.5 Jkg^{-1}K^{-1}, ΔS_m estimated by the TF_MB method for a field change of 0–5 T as a function of the temperature is shown in Fig. 5a. When the temperature is below M_s and in the region where two structures coexists, the values of ΔS_m gradually deviates from those obtained from the Maxwell relation. Nevertheless, a maximum value of -28.9 Jkg^{-1}K^{-1} is still obtained at 221 K.

Large ΔS_m is desirable for magnetic refrigeration but only the reversible contribution to the MCE is reliable. In MnMX alloys, the giant ΔS_m has been extensively reported while the drawback of its irreversibility has been seldom proposed. For most MnMX alloys, due to a large ΔT_{hys}, the MST cannot be induced by cyclic magnetic field, resulting in a low reversible ΔS_m. However, for the optimized sample with $x = 0.10$, we will present that the realization of low ΔT_{hys} can greatly improve the reversibility of magnetic-field-induced MST as well as large MCE. Fig. 6a shows two cyclic M-B curves. The data were recorded in two field cycles isothermally for each measured temperature. Focusing on the second cycle, the sample still displays an obvious magnetic-field-induced first-order

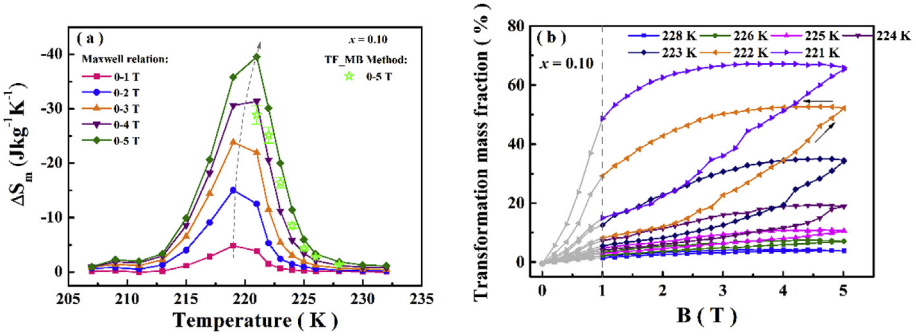

Fig. 5. (a) Magnetic entropy change ΔS_m as a function of temperature under different field change estimated by Maxwell relation. The discrete green stars denote the ΔS_m under 0–5 T field variation obtained by TF_MB method. (b) The transformation mass fraction of the orthorhombic phase as a function of magnetic field during the first cycle. The grey part is excluded due to the numerical instability below 1 T. (For interpretation of the references to colour in this figure legend, the reader is referred to the Web version of this article.)

MST from the hexagonal to the orthorhombic phase which is manifested by a large magnetic hysteresis. In the subsequent cycles, the M-B curves almost overlap with that of the second cycle (See Supplementary Materials, Fig. S5a), indicating a reversible magnetic-field-induced MST. During the increasing field sequence of the second cycle, the magnetization under low field is clearly higher than that during the first cycle. It implies that parts of the magnetic-field-induced orthorhombic phase remains after decreasing the field to zero in the first cycle, while the rest that transforms back to the hexagonal phase can be reproducibly induced by the magnetic field again. This partial reproducible field-induced MST gives rise to the reversible ΔS_m, which can be estimated by the TF_MB method. Fig. 6b and c show the evolution of mass fraction of orthorhombic phase under two magnetic cycles and the corresponding reversible ΔS_m under the magnetic field variation of 0–5 T. There already exists a small number of orthorhombic phase at the start field (1 T) of the first cycle around T_t. While at the initial point of the second cycle, the mass fraction of orthorhombic phase increases and it originates from residual orthorhombic phase upon the removal of field during the first magnetic cycle. With renewed application of magnetic field, for example, the mass fraction can be transformed from 10.9% to 34.6% at 223 K. During this magnetization process, about 23.7% of orthorhombic phase is induced as the reversible part, and it brings about reproducible magnetoresponsive effects. At 222 K, the maximum reversible ΔS_m of -18.6 $Jkg^{-1}K^{-1}$ is achieved. This large value keeps stable in the subsequent cycles (See Supplementary Materials, Fig. S5c). And as shown in Fig. 6d, the magnetic hysteresis loss, which is detrimental to the efficiency of magnetic refrigeration, is reduced during the second field cycle due to the minor loop [19,38]. However, it is essential to further suppress the hysteresis loss to improve the potential of $Mn_{1-x}Fe_{2x}Ni_{1-x}Ge$ as magnetic coolant.

3.5. The origin of low thermal hysteresis

Geometrically nonlinear theory of martensite and the kinematic compatibility have been exploited as a useful strategy tuning phase-transforming materials to low thermal hysteresis and better functional fatigue properties [31,32,40–44]. From the crystallographic theory of martensite, the geometrical compatibility can be improved significantly and the hysteresis is greatly reduced if $\lambda_2 = 1$ where λ_2 is the principal middle eigenvalue of the transformation stretch tensor **U** [40,41,44]. This theory has been successfully used to explain the low ΔT_{hys} in Heusler as well as Ti-Ni-based alloys [6,31,32,38,40,41,43], but whether it can be applied to MnMX system was up to now unexplored. Here, we introduce this theory to the hexagonal MnMX system in which a typical thermoelastic martensitic transition occurs.

According to the crystal relation between orthorhombic and hexagonal structures, the 3×3 transformation stretch tensor **U** is given as below (the detail shown in Supplementary Materials):

$$U = \begin{bmatrix} \frac{b_o}{a_h} & 0 & 0 \\ 0 & \frac{c_o}{\sqrt{3}a_h} & 0 \\ 0 & 0 & \frac{a_o}{c_h} \end{bmatrix} \quad (4)$$

The transformation stretch tensor is diagonal and the universal eigenvalues should be: $\lambda_1 = b_o/a_h < 1$, $\lambda_2 = c_o/(\sqrt{3}a_h)$ and $\lambda_3 = a_o/c_h > 1$, since the MST is accompanied by a large elongation of the a axis and contraction of the b axis of the orthorhombic phase [17]. To accurately obtain the value of λ_2, the sample was cooled to a temperature, at which the hexagonal and the orthorhombic phases coexist,

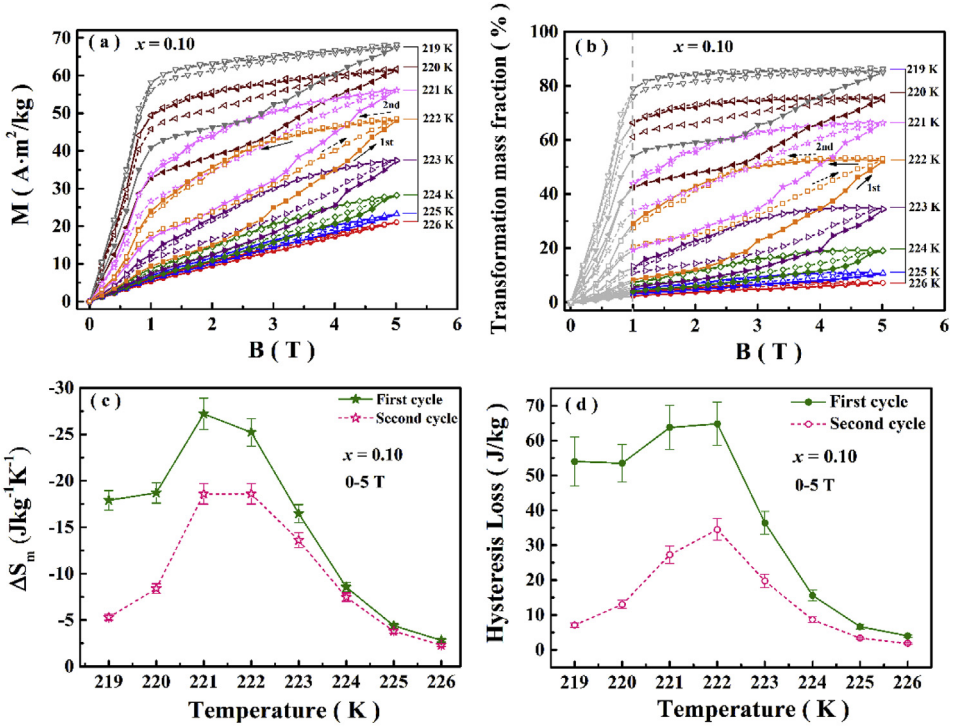

Fig. 6. (a) M-B curves measured during the first (solid line) and second (dashed line) cycle at different temperatures. (b) The evolution of mass fraction of orthorhombic phase under two magnetic field cycles. (c) The ΔS_m under the magnetic field variation of 0–5 T by TF_MB methods during first and second cycles. The ΔS_m during second cycle is reversible. (d) Magnetic hysteresis loss under the magnetic field variation of 0–5 T during first and second cycles.

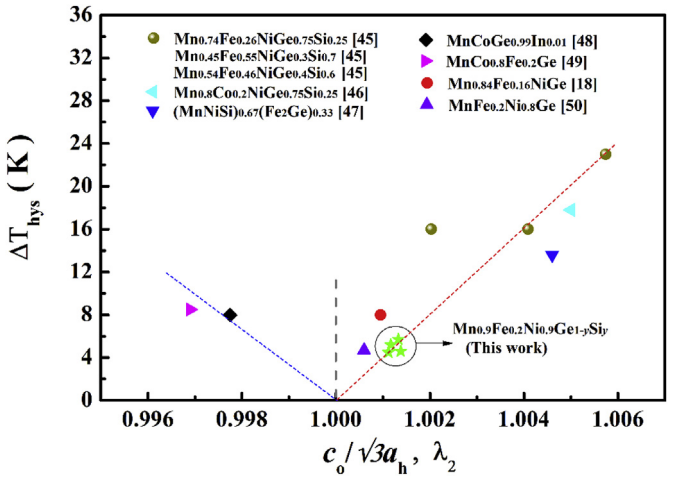

Fig. 7. The relationship between λ_2 and ΔT_{hys} in MnMX alloys. The numbers in the square brackets are the reference numbers [45,46,47,48,49,50].

then XRD measurements were carefully carried out (shown in Fig. S5). The refinement of the XRD patterns indicates that $a_h = 4.09124$ Å and $c_h = 5.34767$ Å for hexagonal phase, while $a_o = 6.00257$ Å, $b_o = 3.74432$ Å and $c_o = 7.09454$ Å for the orthorhombic phase. According to Eq. (4), λ_2 is 1.00117 which is very close to 1. This small value of $|\ 1\text{-}\lambda_2\ |$ indicates that the geometric compatibility of two phases is improved, leading to the realization of low ΔT_{hys} in the $Mn_{0.9}Fe_{0.2}Ni_{0.9}Ge$ sample. Fig. 7 further shows the relationship between λ_2 and ΔT_{hys}. It can be indeed found that ΔT_{hys} in MnMX alloys gradually increases when λ_2 deviates from 1. Generally, the geometrically nonlinear strategy proves that the ΔT_{hys} in MnMX system is determined by the lattice parameter change along the c axis in the orthorhombic phase and a negligible change will result in a low ΔT_{hys}, such as that in this work.

Moreover, the MST with low ΔT_{hys} is not just observed in a single composition, i.e. $Mn_{0.9}Fe_{0.2}Ni_{0.9}Ge$, but tunable in a wide temperature region covering room temperature. Fig. 8a shows the M-T curves for $Mn_{0.9}Fe_{0.2}Ni_{0.9}Ge_{1-y}Si_y$ ($y = 0$, 0.03, 0.05 and 0.10) alloys, which were prepared by the same method mentioned in the experimental part. The introduction of Si increases T_t to be higher than room temperature and keeps ΔT_{hys} nearly unchanged simultaneously. The values of ΔT_{hys} for the samples with $y = 0.03$, 0.05 and 0.10 are 5.7, 4.6 and 4.5 K, respectively. As presented in Figs. 7 and 8b, the obtained low values of ΔT_{hys} are also attributed to λ_2 near one. Thanks to the low ΔT_{hys}, the MSTs in these Si-doped samples can be induced by cyclic magnetic field (Fig. 8c, Fig. S7a and Fig. S7b in Supplementary Materials) and the corresponding maximum values of reversible ΔS_m under a magnetic field variation of 0–5 T increase to −22.8, −22.1 and −24.3 $Jkg^{-1}K^{-1}$ for samples y = 0.03, 0.05 and 0.10, respectively (shown in Fig. 8d).

Fig. 9 shows the reversible ΔS_m for some well-known magnetocaloric materials. Clearly, the reversible ΔS_m in $Mn_{0.9}Fe_{0.2}Ni_{0.9}Ge_{1-y}Si_y$ ($y = 0$, 0.03, 0.05 and 0.10) alloys is comparable with Ni-Mn-based Heusler alloys and La-Fe-Si alloys under a field change of 0–5 T. Nevertheless, it is necessary to point out that under a low field change of 0–2 T, or 0–1 T used in magnetic refrigerator prototypes, the reversible MCE in MnMX would degrade sharply (shown in Fig. S8 in Supplementary Materials). Therefore, enhancing the sensitivity of T_t to magnetic field and further minimizing ΔT_{hys} would be the next step to improve the magnetocaloric performance of MnMX alloys towards practical applications in the future.

4. Conclusion

In summary, we have investigated crystalline structures, microstructures, magnetic properties, transformation behavior and magnetocaloric performance in the low-hysteresis MnNiGe-based system. When Fe is simultaneously introduced into both Mn and Ni

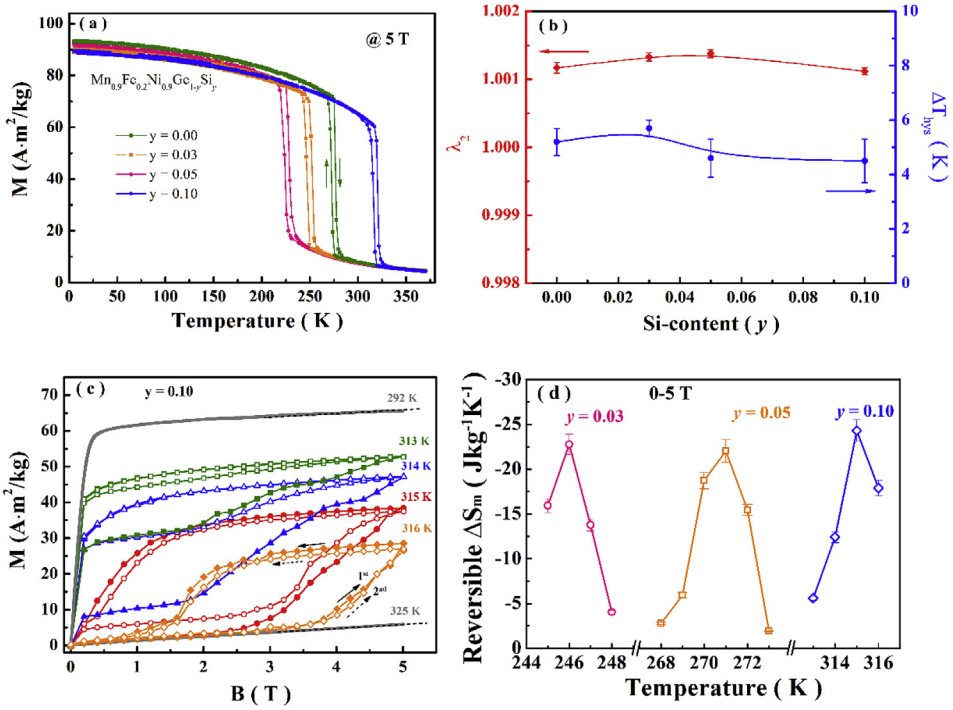

Fig. 8. (a) M-T curves for $Mn_{0.9}Fe_{0.2}Ni_{0.9}Ge_{1-y}Si_y$ ($y = 0$, 0.03, 0.05 and 0.10) alloys. (b) λ_2 and ΔT_{hys} for $Mn_{0.9}Fe_{0.2}Ni_{0.9}Ge_{1-y}Si_y$ alloys. (c) Two cyclic M-B curves for sample $y = 0.10$ around T_t. (d) Reversible ΔS_m under the magnetic field variation of 0–5 T for samples $y = 0.03$, 0.05 and 0.10.

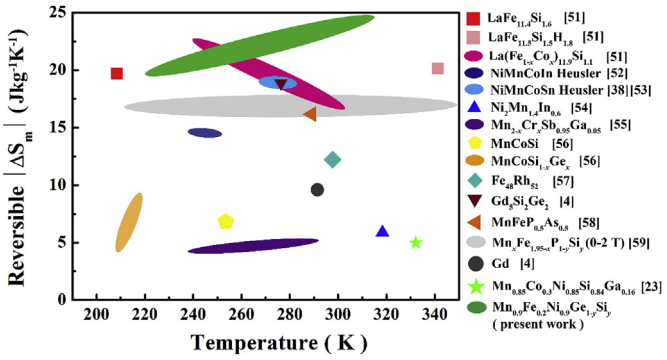

Fig. 9. A statistical graphic of absolute values of reversible ΔS_m under 5 T versus peak temperature for well-known magnetocaloric materials. The numbers in the square brackets are the reference numbers [51,52,53,54,55,56,57,58,59].

sites in MnNiGe alloys, a decrease of T_t and the evolution of ferromagnetism of the orthorhombic phase lead to the achievement of a stable magnetostructural transformation. Through tuning of the composition, a low ΔT_{hys} of 5.2 K together with a large ΔM of 62.1 A m^2/kg is obtained in $Mn_{0.9}Fe_{0.2}Ni_{0.9}Ge$. Due to these optimizations, a partial field-induced MST can reversibly be triggered. Therefore, a reversible magnetocaloric effect with a maximum value of -18.6 Jkg^{-1}K^{-1} is realized with a field variation of 0–5 T. This is the largest value reported in the MnMX system and comparable with many other famous magnetocaloric materials. The observed low ΔT_{hys} in this work is explained based on geometrically nonlinear theory of martensite. Our calculations show that low ΔT_{hys} can be achieved when the lattice parameter change along the *c* axis in the orthorhombic phase is small. Furthermore, the MST with low ΔT_{hys} can be tuned by Si-doping. Therefore, a large reversible MCE can be achieved in a wide range of temperatures covering room temperature. Our work greatly develops the potential of $Mn_{1-x}Fe_{2x}Ni_xGe_{1-y}Si_y$ as a magnetic refrigerant and may open up a way to seek a MnMX alloy exhibiting low hysteresis.

Acknowledgements

The authors would like to thank A. J. E. Lefering and B. Zwart for their technical help. This work was sponsored by the National Natural Science Foundation of China (Grant Nos: 51571121, 51601092 and U1832191), the Natural Science Foundation of Jiangsu Province (Grant No: BK20160833), the Key Research & Development Program of Jiangsu Province (Grant No: BE2017102) and NWO in the Domain Applied and Engineering Sciences (AES) programme. Jun Liu gratefully acknowledges the financial support from China Scholarship Council.

Appendix A. Supplementary data

Supplementary data to this article can be found online at https://doi.org/10.1016/j.actamat.2019.05.066.

References

[1] V. Franco, J.S. Blázquez, J.J. Ipus, J.Y. Law, L.M. Moreno-Ramírez, A. Conde, Magnetocaloric effect: from materials research to refrigeration devices, Prog. Mater. Sci. 93 (2017) 112–232.
[2] O. Gutfleisch, M.A. Willard, E. Brück, C.H. Chen, S.G. Sankar, J.P. Liu, Magnetic materials and devices for the 21st century: stronger, lighter, and more energy efficient, Adv. Mater. 23 (2011) 821–842.
[3] E. Brück, Developments in magnetocaloric refrigeration, J. Phys. D Appl. Phys. 38 (2005) R381–R391.
[4] V.K. Pecharsky, K.A. Gschneidner Jr., Giant magnetocaloric effect in $Gd_5(Si_2Ge_2)$, Phys. Rev. Lett. 78 (1997) 4494–4497.
[5] T. Krenke, E. Duman, M. Acet, E.F. Wassermann, X. Moya, L. Mañosa, A. Planes, Inverse magnetocaloric effect in ferromagnetic Ni-Mn-Sn alloys, Nat. Mat. 4 (2005) 450–454.
[6] J. Liu, T. Gottschall, K.P. Skokov, J.D. Moore, O. Gutfleisch, Giant magnetocaloric effect driven by structural transition, Nat. Mater. 11 (2012) 620–626.
[7] F. Guillou, G. Porcari, H. Yibole, N. van Dijk, E. Brück, Taming the first-order transition in giant magnetocaloric materials, Adv. Mater. 26 (2014) 2671–2675.
[8] X.F. Miao, L. Caron, P. Roy, N.H. Dung, L. Zhang, W.A. Kockelmann, R.A. de Groot, N.H. van Dijk, E. Brück, Tuning the phase transition in transition-metal-based magnetocaloric compounds, Phys. Rev. B 89 (2014) 174429.
[9] F.X. Hu, B.G. Shen, J.R. Sun, Z.H. Chen, G.H. Rao, X.X. Zhang, Influence of negative lattice expansion and metamagnetic transition on magnetic entropy change in the compound $LaFe_{11.4}Si_{1.6}$, Appl. Phys. Lett. 78 (2001) 3675–3677.
[10] A. Fujita, S. Fujieda, Y. Hasegawa, K. Fukamichi, Itinerant-electron metamagnetic transition and large magnetocaloric effects in $La(Fe_xSi_{1-x})_{13}$ compounds and their hydrides, Phys. Rev. B 67 (2003) 104416.
[11] Y.Y. Shao, J. Liu, M.X. Zhang, A.R. Yan, K.P. Skokov, D.Y. Karpenkov, O. Gutfleisch, High-performance solid-state cooling materials: balancing magnetocaloric and non-magnetic properties in dual phase La-Fe-Si, Acta Mater. 125 (2017) 506–512.
[12] N.T. Trung, L. Zhang, L. Caron, K.H.J. Buschow, E. Brück, Giant magnetocaloric effects by tailoring the phase transitions, Appl. Phys. Lett. 6 (2010) 172504.
[13] J. Liu, Y.Y. Gong, G.Z. Xu, G. Peng, I.A. Shah, N. ul Hassan, F. Xu, Realization of magnetostructural coupling by modifying structural transitions in MnNiSi-CoNiGe system with a wide Curie-temperature window, Sci. Rep. 6 (2016) 23386.
[14] C.L. Zhang, D.H. Wang, Q.Q. Cao, Z.D. Han, H.C. Xuan, Y.W. Du, Magneto-structural phase transition and magnetocaloric effect in off-stoichiometric $Mn_{1.9-x}Ni_xGe$ alloys, Appl. Phys. Lett. 93 (2008) 122505.
[15] L. Caron, N.T. Trung, E. Brück, Pressure-tuned magnetocaloric effect in $Mn_{0.93}Cr_{0.07}CoGe$, Phys. Rev. B 84 (2011), 020414(R).
[16] F. Guillou, F. Wilhelm, O. Tegus, A. Rogalev, Microscopic mechanism of the giant magnetocaloric effect in MnCoGe alloys probed by x-ray magnetic circular dichroism, Appl. Phys. Lett. 108 (2016) 122405.
[17] E.K. Liu, W.H. Wang, L. Feng, W. Zhu, G.J. Li, J.L. Chen, H.W. Zhang, G.H. Wu, C.B. Jiang, H.B. Xu, F. de Boer, Stable magnetostructural coupling with tunable magnetoresponsive effects in hexagonal ferromagnets, Nat. Commun. 3 (2012) 873.
[18] A. Kitanovski, J. Tušek, U. Tomc, U. Plaznik, M. Ozbolt, A. Poredoš, Magnetocaloric Energy Conversion: from Theory to Applications, Springer International Publishing, Switzerland, 2015.
[19] T. Gottschall, K.P. Skokov, B. Frincu, O. Gutfleisch, Large reversible magnetocaloric effect in Ni-Mn-In-Co, Appl. Phys. Lett. 106 (2015) 021901.
[20] T. Gottschall, K.P. Skokov, R. Burriel, O. Gutfleisch, On the S (T) diagram of magnetocaloric materials with first-order transition: kinetic and cyclic effects of Heusler alloys, Acta Mater. 107 (2016) 1–8.
[21] E.K. Liu, H.G. Zhang, G.Z. Xu, X.M. Zhang, R.S. Ma, W.H. Wang, J.L. Chen, H.W. Zhang, G.H. Wu, L. Feng, X.X. Zhang, Giant magnetocaloric effect in isostructural MnNiGe-CoNiGe system by establishing a Curie-temperature window, Appl. Phys. Lett. 102 (2013) 122405.
[22] D. Kasimov, J. Liu, Y.Y. Gong, G.Z. Xu, F. Xu, G.W. Lu, Realization of magnetostructural coupling in a high temperature region in $Mn_{0.85}Co_{0.3}Ni_{0.85}Si_{1-x}Ga_x$ system, J. Alloy. Comp. 733 (2018) 15–21.
[23] W. Bażela, A. Szytuła, J. Todorović, Z. Tomkowicz, A. Zięba, Crystal and magnetic structure of NiMnGe, Phys. Status Solidi A 38 (1976) 721–729.
[24] H. Fjellvåg, A.F. Andresen, On the crystal structure and magnetic properties of MnNiGe, J. Magn. Magn. Mater. 50 (1985) 291–297.
[25] T. Roisnel, J. Rodríquez-Carvajal, WinPLOTR: a windows tool for powder diffraction pattern analysis, Mater. Sci. Forum 378 (2001) 118–123.
[26] L. Caron, Z.Q. Ou, T.T. Nguyen, D.T. Cam Thanh, O. Tegus, E. Brück, On the determination of the magnetic entropy change in materials with first-order transitions, J. Magn. Magn. Mater. 321 (2009) 3559–3566.
[27] T. Samanta, I. Dubenko, A. Quetz, J. Prestigiacomo, P.W. Adams, S. Stadler, N. Ali, $Mn_{1-x}Fe_xCoGe$: a strongly correlated metal in the proximity of a noncollinear ferromagnetic state, Appl. Phys. Lett. 103 (2013) 042408.
[28] W. Jeitschko, A high-temperature X-ray study of the displacive phase transition in MnCoGe, Acta Crystallogr. B31 (1975) 1187–1190.
[29] J.T. Wang, D.S. Wang, C. Chen, O. Nashima, T. Kanomata, H. Mizuseki, Y. Kawazoe, Vacancy induced structural and magnetic transition in $MnCo_{1-x}Ge$, Appl. Phys. Lett. 89 (2006) 262504.
[30] N. ul Hassan, F.H. Chen, M.G. Zhang, I.A. Shah, J. Liu, Y.Y. Gong, G.Z. Xu, F. Xu, Realisation of magnetostructural coupling and a large magnetocaloric effect in the $MnCoGe_{1+x}$ system, J. Magn. Magn. Mater. 439 (2017) 120–125.
[31] V. Srivastava, X. Chen, R.D. James, Hysteresis and unusual magnetic properties in the singular Heusler alloy $Ni_{45}Co_5Mn_{40}Sn_{10}$, Appl. Phys. Lett. 97 (2010) 014101.
[32] D.W. Zhao, J. Liu, X. Chen, W. Sun, Y. Li, M.X. Zhang, Giant caloric effect of low-hysteresis metamagnetic shape memory alloys with exceptional cyclic functionality, Acta Mater. 133 (2017) 217–223.
[33] T. Samanta, I. Dubenko, A. Quetz, S. Temple, S. Stadler, N. Ali, Magneto-structural phase transitions and magnetocaloric effects in $MnNiGe_{1-x}Al_x$, Appl. Phys. Lett. 100 (2012) 052404.
[34] E.K. Liu, Y. Du, J.L. Chen, W.H. Wang, H.W. Zhang, G.H. Wu, Magnetostructural transformation and magnetoresponsive properties of $MnNiGe_{1-x}Sn_x$ alloys,

IEEE Trans. Magn. 47 (2010) 4041–4043.
[35] G.J. Liu, J.R. Sun, J. Shen, B. Gao, H.W. Zhang, F.X. Hu, B.G. Shen, Determination of the entropy changes in the compounds with a first-order magnetic transition, Appl. Phys. Lett. 90 (2007) 032507.
[36] V. Basso, C.P. Sasso, K.P. Skokov, O. Gutfleisch, V.V. Khovaylo, Hysteresis and magnetocaloric effect at the magnetostructural phase transition of Ni-Mn-Ga and Ni-Mn-Co-Sn Heusler alloys, Phys. Rev. B 85 (2012) 014430.
[37] J.S. Blázquez, V. Franco, A. Conde, T. Gottschall, K.P. Skokov, O. Gutfleisch, A unified approach to describe the thermal and magnetic hysteresis in Heusler alloys, Appl. Phys. Lett. 109 (2016) 122410.
[38] Y.H. Qu, D.Y. Cong, X.M. Sun, Z.H. Nie, W.Y. Gui, R.G. Li, Y. Ren, Y.D. Wang, Giant and reversible room-temperature magnetocaloric effect in Ti-doped Ni-Co-Mn-Sn magnetic shape memory alloys, Acta Mater. 134 (2017) 236–248.
[39] M.D. Kuz'min, Shape of temperature dependence of spontaneous magnetization of ferromagnets: quantitative analysis, Phys. Rev. Lett. 94 (2005) 107204.
[40] J. Cui J, Y.S. Chu, O. Famodu, Y. Furuya, J. Hattrick-Simpers, R.D. James, A. Ludwig, S. Thienhuas, M. Wutting, Z. Zhang, I. Takechi, Combinatorial search of thermoelastic shape-memory alloys with extremely small hysteresis width Combinatorial search of thermoelastic shape-memory alloys with extremely small hysteresis width, Nat. Mater. 5 (2006) 286–290.
[41] Z. Zhang, R.D. James, S. Müller, Energy barriers and hysteresis in martensitic phase transformations, Acta Mater. 57 (2009) 4332–4352.
[42] Y. Song, X. Chen, V. Dabade, T.W. Shield, R.D. James, Enhanced reversibility and unusual microstructure of a phase-transforming material, Nature 502 (2013) 85–88.
[43] C. Chluba, W. Ge, R. L de Miranda, J. Strobel, L. Kienle, E. Quandt, M. Wuttig, Ultralow-fatigue shape memory alloy films, Science 348 (2015) 1004–1007.
[44] X. Chen, Y. Song, N. Tamura, R.D. James, Determination of the stretch tensor for structural transformations, J. Mech. Phys. Solids 93 (2016) 34–43.. Transformation stretch tensor can be calculated by STRUCTRANS on, http://www.structrans.org/#/.
[45] Z.Y. Wei, E.K. Liu, Y. Li, G.Z. Xu, X.M. Zhang, G.D. Liu, X.K. Xi, H.W. Zhang, W.H. Wang, G.H. Wu, X.X. Zhang, Unprecedentedly wide Curie-temperature windows as phase-transition design platform for tunable magneto-multifunctional materials, Adv. Electron. Mater. 1 (2015) 1500076.
[46] Y. Li, Z.Y. Wei, H.G. Zhang, E.K. Liu, H.Z. Luo, G.D. Liu, X.K. Xi, S.G. Wang, W.H. Wang, M. Yue, G.H. Wu, X.X. Zhang, Windows open for highly tunable magnetostructural phase transitions, Apl. Mater. 4 (2016) 071101.
[47] C.L. Zhang, H.F. Shi, E.J. Ye, Y.G. Nie, Z.D. Han, B. Qian, D.H. Wang, Magneto-structural transition and magnetocaloric effect in MnNiSi-Fe2Ge system, Appl. Phys. Lett. 107 (2015) 212403.
[48] R.R. Wu, L.F. Bao, F.X. Hu, H. Wu, Q.Z. Huang, J. Wang, X.L. Dong, G.N. Li, J.R. Sun, F.R. Shen, T.Y. Zhao, X.Q. Zheng, L.C. Wang, Y. Liu, W.L. Zuo, Y.Y. Zhao, M. Zhang, X.C. Wang, C.Q. Jin, G.H. Rao, X.F. Han, B.G. Shen, Giant barocaloric effect in hexagonal Ni_2In-type Mn-CoGe-In compounds around room temperature, Sci. Rep. 5 (2015) 18027.
[49] J.X. Zeng, Z.L. Wang, Z.H. Nie, Y.D. Wang, Crystal structural transformation accompanied by magnetic transition in $MnCo_{1-x}Fe_xGe$ alloys, Intermetallics 52 (2014) 101–104.
[50] E.K. Liu, Z.Y. Wei, Y. Li, G.D. Liu, H.Z. Luo, W.H. Wang, H.W. Zhang, G.H. Wu, A coupling of martensitic and metamagnetic transitions with collective magnetovolume and table-like magnetocaloric effects, Appl. Phys. Lett. 105 (2014) 062401.
[51] B.G. Shen, J.R. Sun, F.X. Hu, H.W. Zhang, Z.H. Cheng, Recent progress in exploring magnetocaloric materials, Adv. Mater. 21 (2009) 4545–4564.
[52] L. Huang, D.Y. Cong, L. Ma, Z.H. Nie, Z.L. Wang, H.L. Suo, Y. Ren, Y.D. Wang, Large reversible magnetocaloric effect in a Ni-Co-Mn-In magnetic shape memory alloy, Appl. Phys. Lett. 108 (2016) 032405.
[53] Y.H. Qu, D.Y. Cong, S.H. Li, W.Y. Gui, Z.H. Nie, M.H. Zhang, Y. Ren, Y.D. Wang, Simultaneously achieved large reversible elastocaloric and magnetocaloric effects and their coupling in a magnetic shape memory alloy, Acta Mater. 151 (2018) 41–55.
[54] S. Singh, L. Caron, S.W. D'Souza, T. Fichtner, G. Porcari, S. Fabbrici, C. Shekhar, S. Chadov, M. Solzi, C. Felser, Large magnetization and reversible magnetocaloric effect at the second-order magnetic transition in heusler materials, Adv. Mater. 28 (17) (2016) 3321–3325.
[55] A. Tekgül, M. Acet, F. Scheibel, M. Farle, N. Ünal, The reversibility of the inverse magnetocaloric effect in $Mn_{2-x}Cr_xSb_{0.95}Ga_{0.05}$, Acta Mater. 124 (2017) 93–99.
[56] K.G. Sandeman, R. Daou, S. Özcan, J.H. Durrell, N.D. Mathur, D.J. Fray, Negative magnetocaloric effect from highly sensitive metamagnetism in $CoMnSi_{1-x}Ge_x$, Phys. Rev. B 74 (2006) 224436.
[57] M. Manekar, S.B. Roy, Reproducible room temperature giant magnetocaloric effect in Fe-Rh, J. Phys. D Appl. Phys. 41 (2008) 192004.
[58] R. Szymczak, N. Nedelko, S. Lewińska, E. Zubov, A. Sivachenko, I. Gribanov, I. Radelytskyi, K. Dyakonov, A. Ślawska-Waniewska, V. Valkov, V. Varyukhin, V. Dyakonov, H. Szymczak, Comparison of magnetocaloric properties of the $Mn_{2-x}Fe_xP_{0.5}As_{0.5}$ (x = 1.0 and 0.7) compounds, Solid State Sci. 36 (2014) 29–34.
[59] N.H. Dung, Z.Q. Ou, L. Caron, L. Zhang, D.T.C. Thanh, G.A. de Wijs, R.A. de Groot, K.H.J. Buschow, E. Brück, Mixed magnetism for refrigeration and energy conversion, Adv. Energy Mater. 1 (2011) 1215–1219.